Journal of Ceramic Processing Research. Vol. 20, No. 2, pp. 169~172 (2019)

J O U R N A L O F
Ceramic Processing Research

Controlled infiltration profile of SiC coating layer on graphite by Si vapor deposition reaction

Kuk-Jin Hwang[a,b], Kyoung-Ho Kim[a,b], Yoon-Cheol Lee[c], Jung-Tae Hwang[c], Heesoo Lee[b], Seong-Min Jeong[a], Myung-Hyun Lee[a] and Si-Young Bae[a,*]

[a]*Energy and Environmental Division, Korea Institute of Ceramic Engineering and Technology, Jinju-si Gyeongsangnam-do 52851, Korea*

[b]*Department of Materials Science and Engineering, Pusan National University, Busan 609-735, Korea*

[c]*Genecoat, Hwaseong-si Gyeonggi-do 18487, Korea*

SiC-coated graphite was successfully fabricated at different temperatures (1300-1600 ºC) through a silicon vapor deposition reaction (Si-VDR) process. Si powder was used for the Si source of the SiC coating layers. When Si powder was evaporated at high temperature near the melting point of bulk Si, Si gases are moved and changed into Si liquid at the surface of the graphite. The high-temperature process facilitated the formation of SiC coating layers on the graphite. The microstructural, mechanical, and thermal oxidation properties of the coated graphite were investigated.

Keywords: Graphite, Silicon vapor deposition reaction (Si-VDR), Silicon carbide, Oxidation.

Introduction

Graphite is conventionally used for applications such as electronic and energy-related devices, owing to its excellent physical and chemical properties: good heat resistance, corrosion resistance, electrical conductivity, lubricity, workability, and high-temperature strength [1]. Recently, graphite has been developed for functional susceptors in high-temperature processes (e.g., graphite molds have been used to fabricate a curved glass [2,3], which is applied to solar cells and smart IT devices).

Graphite consists of many graphene layers, which are maintained by weak van der Waals forces. This unique structure leads to the formation of significant dust during the mechanical processing of graphite [4, 5]. Moreover, graphite undergoes oxidation at high temperatures [6]. These drawbacks must be overcome to allow the use of graphite as functional susceptors in industry. Methods for depositing a SiC coating on graphite have recently been developed. Compared with graphite, SiC has a similar thermal expansion coefficient, but is characterized by better oxidation resistance and mechanical properties [6]. Hence, SiC coating layers compensate for the drawbacks of graphite.

SiC-coated graphite has been prepared via: chemical vapor deposition (CVD) [6,7], molecular beam epitaxy (MBE) [8], and pack-cementation methods [9]. In the case of CVD, organic precursors such as methyltrichlorosilane (CH_3SiCl_3) have been used for the deposition of SiC layers on graphite [7]. Chlorine-based precursors yield a high growth rate of SiC layers, but generate toxic gases (e.g., HCl) and result in corrosion of the apparatus during the process. High-quality SiC layers can be grown via MBE [8], but the deposition thickness is limited due to the low growth rate. Mixture powders containing Si, SiC, SiO_2, and Al_2O_3 are used for the Si gas source in the pack-cementation method [9]. However, control of the deposition parameters associated with the optical deposition of SiC layers is difficult.

In this study, we report the preparation of SiC-coated graphite through a silicon-based vapor deposition reaction (VDR) process. The temperature-dependent SiC-coated behaviors were analyzed and the fabrication mechanism of SiC-coated graphite was discussed. The microstructural properties and thermal oxidation resistances were also investigated, to elucidate the suitability of the VDR process for mechanical applications.

Experimental Procedure

Silicon powders (purity >99%, Korea Metal Silicon, Korea) were placed at the center of a box furnace (Fig. 1). SiC-layer deposition was performed at pressures lower than 10^{-1} Torr under Ar gas atmosphere. The temperature was maintained at 1300-1600 ºC for 30 min. Graphite (Ellor 40, Mersen, USA), maintained at 100-200 ºC lower than the reaction temperature, was

*Corresponding author:
Tel : +82-55-792-2574
Fax: +82-55-792-2580
E-mail: sybae@kicet.re.kr

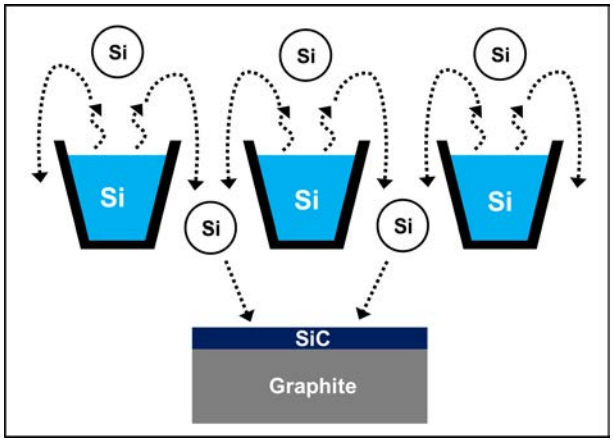

Fig. 1. Schematic of the experimental setup for the Si-VDR process.

then placed on the region.

The microstructural and morphological properties of the samples were characterized via X-ray diffraction (XRD, D/MAX 2200V/PC, Rigaku, Japan), micro-Raman spectroscopy (α-300, WITec, Germany; wavelength: 532 nm), field-emission scanning electron microscopy (FESEM, JSM-6700F, JEOL, Japan) combined with energy-dispersive X-ray spectroscopy (EDS), and optical microscopy (ME600, Nikon, Japan). Nanoindentation measurements (Nano Hardness Tester, CSM instruments, Switzerland) were performed at maximum loads of ~5 mN using a diamond Berkovich pyramid tip. In preparation for SEM, samples were polished with different grades of sandpaper (800, 1200, and 2000).

Results and Discussion

Fig. 2 shows optical micrographs of the graphite surfaces before (Fig. 2(a)) and after Si-VDR (Fig. 2(b)). The pre-Si-VDR graphite commonly shows a high density of surface defects, such as scratches and pores (some with sizes of >50 μm), as indicated in Fig. 2(a). These defects are almost inevitable due to mechanically detrimental processing, e.g., slicing and milling, of the graphite blocks. However, the rough surfaces became relatively smooth after being covered by the SiC layer, as shown in Fig. 2(b). The phase composition of the layer was determined via XRD scans (see Fig. 3) of the graphite and the SiC/graphite composite. For the graphite, several peaks corresponding to (002), (020), (111), (004), and (200) crystal planes occurred at 2θ values of 26.7 °, 42.4 °, 44.7 °, 55.1 °, and 77.6 °, respectively. In addition to the inherent peaks of graphite, peaks associated with the (111), (220), and (311) crystal planes of the cubic β-SiC (JCPDS no. 73-1708) comprising the SiC/graphite composite were also observed. These peaks occurred at 2θ values of 35.8 °, 60.2 °, and 72.0 °, respectively. Owing to the thinness

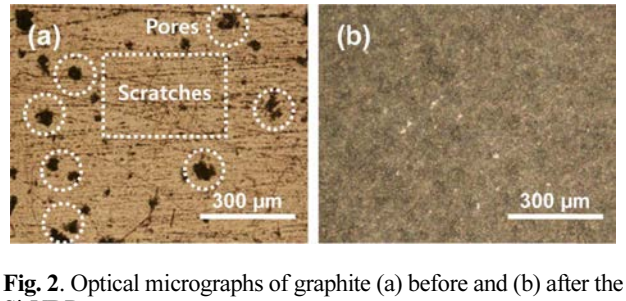

Fig. 2. Optical micrographs of graphite (a) before and (b) after the Si-VDR process.

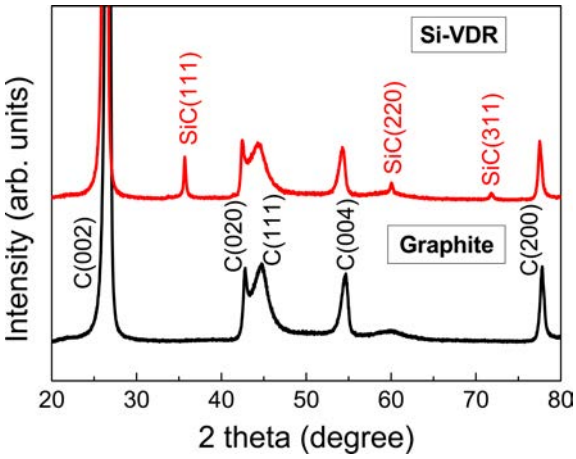

Fig. 3. The XRD of the original graphite block and the SiC-coated graphite.

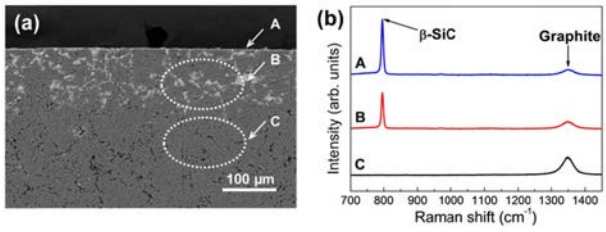

Fig. 4. (a) Cross-sectional FE-SEM image and (b) Raman spectra of SiC-coated graphite prepared at 1300°C.

of the coated layer (thickness: <10 μm), the intensity resulting from the β-SiC layer was lower than those of the graphite peaks.

Fig. 4(a) shows a cross-sectional SEM image of the SiC/graphite composite. The thickness of the topmost SiC layer (denoted as region A) was ~10 μm. Regions consisting of SiC components appeared in bright contrast, owing to the presence of different elements, which were randomly spread from top-to-bottom, as shown in region B. The deep regions of the graphite (region C) consisted of pores only rather than SiC-related components, indicating that the vaporized Si infiltrated the graphite by filling the pores. The local phase properties of the SiC/graphite in regions A-C were determined via micro-Raman spectroscopy (see corresponding results in Fig. 4(b)). As the figure shows, the β-SiC component occurred in regions A and B and

was characterized by a Raman shift of 795.8 cm^{-1}. However, an intense graphite peak (Raman shift: 1348.0 cm^{-1}) occurred only in region C. The peak ratio between SiC and graphite indicates that the amount of SiC component decreased gradually from the top of the graphite to the bottom.

The infiltration behavior of vaporized Si in a SiC/graphite composite was investigated via EDS analysis (see Fig. 5(a) for an EDS mapping image of elemental Si). As the Raman analysis revealed, the distribution of Si is directly correlated with the formation of SiC. The temperature dependence of the infiltration depth was investigated through a VDR process performed at temperatures ranging from 1300 to 1600 °C. Here, the Si content was deduced from the image processing software (Image-Pro 6.2, MediaCybernetics, Korea). The results revealed that the Si content, which was highest in the sub-surface regions, decreased sharply from the top to the bottom of the SiC/graphite composite, as shown in Fig. 5(b). The effective thickness of the deposited SiC layer was estimated via linear fitting of each curve. This procedure yielded effective thickness of values of 22, 22, 50, and 70 μm for the SiC layer fabricated at 1300, 1400, 1500, and 1600 °C, respectively. In other words, the thickness of the layer increased with increasing VDR temperature. Furthermore, a residual amount of Si (at a depth of 150 μm) decreased with increasing VDR temperature. This indicates that the pores, which served as a route for Si infiltration, were rapidly blocked at high processing temperatures, leading to thickening of the SiC layer with increasing processing time. However, prolonged Si infiltration occurred at low processing temperature, resulting in relatively high Si content in the deep regions of the SiC/graphite composite.

The aforementioned results revealed the formation mechanism of SiC layers generated via the Si-VDR method. The Si-VDR process consists of the following steps (see Fig. 6): i) evaporated Si(*g*) reaches the surface of graphite, ii) Si(*g*) infiltrates the pores of graphite and is partially condensed (Si(*l*)), iii) diffusion of C(*s*) from graphite at high temperature, is accompanied by the formation of SiC(*s*), iv) the pores are filled with SiC(*s*), and the corresponding channel is blocked. The reactions between Si and C are given as follows:

$$Si(l) + C(s) \rightarrow SiC(s) \quad (1)$$
$$Si(l) + C(s) \rightarrow Si/C(soln.) \quad (2)$$
$$Si/C(soln.) \rightarrow SiC(s) \quad (3)$$

C has a low solubility (~0.5%) in Si [11]. However, the dissolution of C in Si is exothermic (eq. (1)). Owing to the increase in the local temperature of the adjacent region (eq. (2)), this reaction yields increased C solubility in Si. The formation of solid SiC from dissolved Si/C is thereby promoted (eq. (3)).

The thermal durability of the SiC/graphite composites

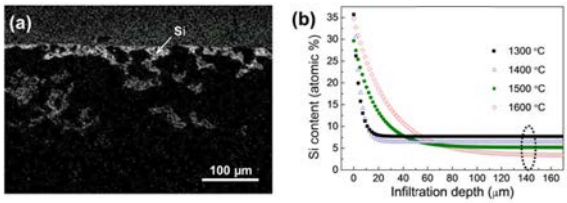

Fig. 5. (a) EDS mapping images of SiC-coated graphite and (b) Si content as a function of the cross-sectional infiltration depth.

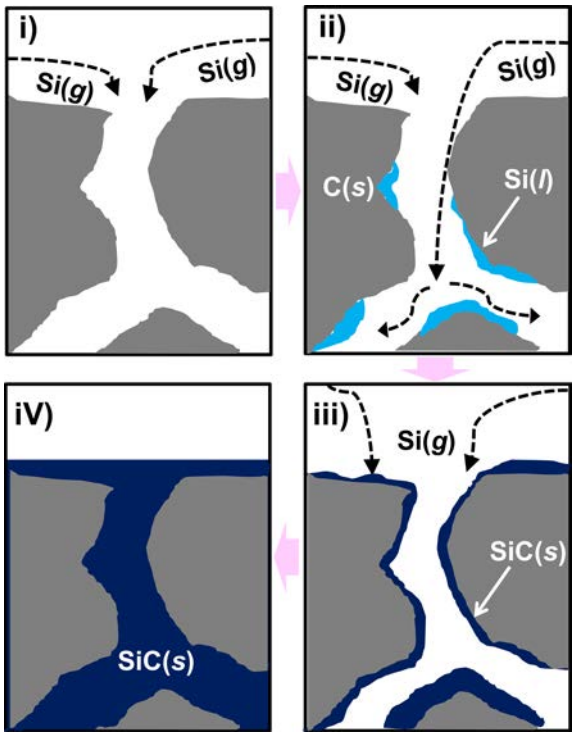

Fig. 6. Schematic of SiC formation during the Si-VDR process: i) Si(*g*) arrival at the surface, ii) infiltration and partial condensation, iii) beginning of SiC(*s*) formation, and iv) SiC(*s*) pore filling.

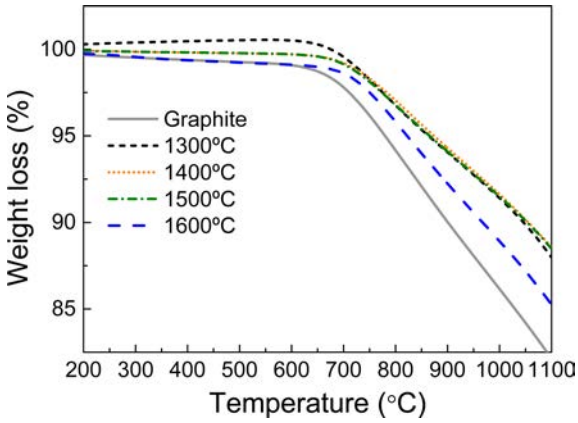

Fig. 7. Weight change of the SiC-coated graphite as a function of the temperature.

was investigated via thermal gravity analysis (TGA; see Fig. 7 for the weight loss of the composites as a function

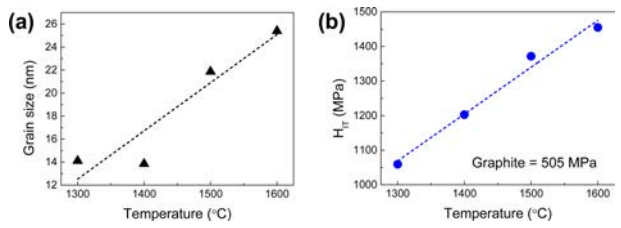

Fig. 8. Temperature dependence of the grain size and hardness of the SiC-coated graphite.

of the temperature). Several composites were prepared at various VDR processing temperatures. Each sample underwent rapid weight loss at temperatures ranging from ranging from 600 to 800 °C. In particular, compared with the weight loss of the SiC/graphite composite, the weight loss of bare graphite decreased sharply, owing to severe thermal oxidation behaviors. Hence, by reducing the carbon oxidation, the SiC coating resulted in considerable enhancement of the thermal durability. This indicated that the relatively rapid weight loss of the composite fabricated at 1600 °C is related to the small high-temperature infiltration depth of Si. The weight loss determined via TGA is isotropic. This explains the rapid weight loss of the sample grown at 1600 °C, where the oxidation is isotropic for all directions, except the surface normal direction.

The results revealed that the high temperature of the VDR process inhibited the infiltration of Si and, hence, SiC was formed mainly on the surface. Furthermore, the SiC layer was formed at various temperatures and, correspondingly, temperature-dependent surface properties were expected. Fig. 8(a) shows the temperature dependence of the grain size (B), which was calculated from the XRD results, using Scherrer's equation:

$$B = \frac{K\lambda}{L\cos\theta} \quad (4)$$

where, K, λ, L, and θ are a constant, the X-ray wavelength, full width at half maximum, and angle of the XRD peak, respectively. The grain size increased (from 14 nm to 26 nm) with increasing growth temperature. In other words, high thermal energy facilitates the growth of SiC grains. Fig. 8(b) shows the hardness of the SiC/graphite composite as a function of the temperature. The hardness was also measured via nanoindentation of the SiC surface. The results revealed that the hardness of the samples increased (in general) with increasing temperature, i.e., values of 1059.5 MPa (1300 °C), 1202.9 MPa (1400 °C), 1371.7 MPa (1500 °C), and 1455.0 MPa (1600 °C) were obtained. In general, the hardness of large grains (>100 nm) is inversely proportional to the grain size [12]. However, in this experiment, the maximum size of a SiC grain was lower than 26 nm. The enhancement in the hardness might be strongly influenced by the increased thickness of the SiC coating layer.

Conclusions

In the VDR process, high-temperature (>1300°C) thermal evaporation of Si, was followed by reaction of Si with graphite and, in turn, formation of SiC/graphite composites. The SiC components were formed via the infiltration of pores in the graphite. However, the infiltration depth decreased with increasing growth temperature (owing to the rapid blocking of the pores), whereas the thickness and grain size of the SiC coating layers increased. The hardness was enhanced by the coating, and was adjustable depending on the growth temperature. Therefore, the VDR process represents a quite promising method for SiC-layer formation on and, hence, improved mechanical hardness as well as oxidation resistance of graphite.

Acknowledgements

This work was supported by the Technology Innovation Program (No. 10053062) funded by the Ministry of Trade, Industry & Energy (MI, Korea)

References

1. M.S. Dresselhaus and G. Dresselhaus, Adv. Phys. 30 (1981) 139-326.
2. L.M. Cook, J. Non-crystalline Solids 120 (1990) 152-171.
3. T. Saito, A. Shimura and S. Ichikawa, Sol. Energ. Mat. 9 (1983) 337-345.
4. L. Xiaowei, R. Jean-Charles and Y. Suyuan, Nuc. Eng. and Design 227 (2004) 273-280.
5. E.L. Fuller and J.M. Okoh, J. Nuc. Mat. 240 (1997) 241-250.
6. X. Yang, Q. Z. Huang, Z. Su, X. Chang, L. Y. Chai, C. X. Liu, L. Xue, D. Huang, Corros. Sci. 75 (2013) 16-27.
7. Y. Liu, L. Cheng, L. Zhang, S. Wu, D. Li and Y. Xu, Mater. Sci. Eng. 466 (2007) 172-177.
8. M.E. Lin, B. Sverdlov, G.L. Zhou and H. Morkoç, Appl. Phys. Lett. 62 (1993) 3479-3481.
9. Q.G. Fu, H.J. Li, X.H. Shi, K.Z. Li and G.D. Sun, Scripta Mater. 52 (2005) 923-927.
10. J. Wasyluk, T. S. Perova, S.A. Kukushkin, A.V. Osipov, N.A. Feoktistov, and S.A. Grudinkin, Mater. Sci. Forum 645 (2010) 359-362.
11. J.N. Ness, and T.F. Page, J. Mat. Sci. 21 (1986) 1377-1397.
12. H. Gleiter, Acta Mater. 48 (2000) 1-28.